Phonon thermal conductivity suppression of bulk silicon nanowire composites for efficient thermoelectric conversion

Ting-Gang Chen,[1] Peichen Yu,[1,*] Rone-Hwa Chou,[2] and Ci-Ling Pan[2]

[1]*Department of Photonics and Institute of Electro-Optical Engineering, National Chiao Tung University, Hsinchu, Taiwan*

[2]*Department of Physics, National Tsing Hua University, Hsinchu Taiwan*

**yup@faculty.nctu.edu.tw*

Abstract: Vertically-aligned silicon nanowires (SiNWs) that demonstrate reductions of phonon thermal conductivities are ideal components for thermoelectric devices. In this paper, we present large-area silicon nanowire arrays in various lengths using a silver-induced, electroless-etching method that is applicable to both n- and p-type substrates. The measured thermal conductivities of nanowire composites are significantly reduced by up to 43%, compared to that of bulk silicon. Detailed calculations based on the series thermal resistance and phonon radiative transfer models confirm the reduction of thermal conductivity not only due to the increased air fraction, but also the nanowire size effect, suggesting the soundness of employing bulk silicon nanowire composites as efficient thermoelectric materials.

OCIS codes: (160.4236) Nanomaterials; (120.6810) Thermal effects; (030.5620) Radiative transfer; (130.1750) Components.

References and links

1. F. J. DiSalvo, "Thermoelectric cooling and power generation, " Science **285**(5428), 703–706 (1999).
2. G. S. Nolas, J. Sharp, and H. Goldsmid, Thermoelectrics: Basic Principles and New Materials Developments, Springer, New York (2001).
3. G. A. Slack, CRC Handbook of Thermoelectrics, D. M. Rowe Ed., Boca Raton, Florida, (1995).
4. R. Venkatasubramanian, "Recent Trends in Thermoelectric Materials Research III, in Semiconductors and Semimetals," Academic Press **71**, 175–201 (2001).
5. G. Chen, "Recent Trends in Thermoelectric Materials Research III, in Semiconductors and Semimetals," Academic Press **71**, 203–259 (2001).
6. R. Venkatasubramanian, E. Siivola, T. Colpitts, and B. O'Quinn, "Thin-film thermoelectric devices with high room-temperature figures of merit," Nature **413**(6856), 597–602 (2001).
7. S. M. Lee, D. G. Cahill, and R. Venkatasubramanian, "Thermal conductivity of Si-Ge superlattices," Appl. Phys. Lett. **70**(22), 2957–2959 (1997).
8. A. I. Hochbaum, R. Chen, R. D. Delgado, W. Liang, E. C. Garnett, M. Najarian, A. Majumdar, and P. Yang, "Enhanced thermoelectric performance of rough silicon nanowires," Nature **451**(7175), 163–167 (2008).
9. A. I. Boukai, Y. Bunimovich, J. Tahir-Kheli, J.-K. Yu, W. A. Goddard 3rd, and J. R. Heath, "Silicon nanowires as efficient thermoelectric materials," Nature **451**(7175), 168–171 (2008).
10. K. Q. Peng, Y. J. Yan, S. P. Gao, and J. Zhu, "Synthesis of Large-Area Silicon Nanowire Arrays via Self-Assembling Nanoelectrochemistry," Adv. Mater. **14**(16), 1164–1167 (2002).
11. K. Q. Peng, Y. Yan, S. P. Gao, and J. Zhu, "Dendrite-Assisted Growth of Silicon Nanowires in Electroless Metal Deposition," Adv. Funct. Mater. **13**(2), 127–132 (2003).
12. Y.-F. Huang, S. Chattopadhyay, Y.-J. Jen, C.-Y. Peng, T.-A. Liu, Y.-K. Hsu, C.-L. Pan, H.-C. Lo, C.-H. Hsu, Y.-H. Chang, C.-S. Lee, K.-H. Chen, and L.-C. Chen, "Improved broadband and quasi-omnidirectional anti-reflection properties with biomimetic silicon nanostructures," Nat. Nanotechnol. **2**(12), 770–774 (2007).
13. W. J. Parker, R. J. Jenkins, C. P. Butler, and G. L. Abbott, "Flash method of determining thermal diffusivity, heat capacity, and thermal conductivity," J. Appl. Phys. **32**(9), 1679–1684 (1961).
14. D. G. Cahill, "Thermal conductivity measurement from 30~750K: the 3ω method," Rev. Sci. Instrum. **61**(2), 802–808 (1990).
15. S. Mo, P. Hu, J. Cao, Z. Chen, H. Fan, and F. Yu, "Effective Thermal Conductivity of Moist Porous Sintered Nickel Material," Int. J. Thermophys. **27**(1), 304–313 (2006).
16. J. L. Zeng, Z. Cao, D. W. Yang, L. X. Sun, and L. Zhang, "Thermal conductivity enhancement of Ag nanowires on an organic phase change material," J. Therm. Anal. Calorim. (to be published).

#131401 - $15.00 USD Received 13 Jul 2010; revised 3 Sep 2010; accepted 3 Sep 2010; published 9 Sep 2010

17. H. Wang, J. Y. Feng, X. J. Hu, and K. M. Ng, "Reducing thermal contact resistance using a bilayer aligned CNT thermal interface material," Chem. Eng. Sci. **65**(3), 1101–1108 (2010).
18. Y. He, "Rapid thermal conductivity measurement with a hot disk sensor Part 1. Theoretical considerations," Thermochim. Acta **436**(1-2), 122–129 (2005).
19. G. Chen, "Thermal conductivity and ballistic-phonon transport in the cross-plane direction of superlattices," Phys. Rev. B **57**(23), 14958–14973 (1998).
20. K. Miyazaki, T. Arashi, D. Makino, and H. Tsukamoto, "Heat Conduction in Microstructured Materials," IEEE Trans. Compon. Packag. Tech. **29**(2), 247–253 (2006).
21. S. Sihn, and K. Ajit, Roy, "Nanoscale Heat Transfer using Phonon Boltzmann Transport Equation," COMSOL Conference (2009).
22. B. Yang, and G. Chen, "Lattice Dynamics Study Of Anisotropic Heat Conduction in Superlattices," Microscale Thermophys. Eng. **5**(2), 107–116 (2001).
23. G. Chen, and M. Neagu, "Thermal Conductivity and Heat Transfer in Superlattices," Appl. Phys. Lett. **71**(19), 2761–2763 (1997).
24. J. M. Ziman, "Electrons and Phonons," Oxford University Press, London, (1985).
25. D. Terris, K. Joulain, D. Lacroix, and D. Lemonnier, "Numerical simulation of transient phonon heat transfer in silicon nanowires and nanofilms," J. Phys.: Conf. Ser. **92**, 012077 (2007).
26. H. Y. Chen, H. W. Lin, C. Y. Wu, W. C. Chen, J. S. Chen, and S. Gwo, "Gallium nitride nanorod arrays as low-refractive-index transparent media in the entire visible spectral region," Opt. Express **16**(11), 8106–8116 (2008).

1. Introduction

Efficient thermoelectric energy conversion promises a number of applications in modern life. In particular, solid-state cooling and waste-heat harvesting are of tremendous interests to the current IC and embedded systems industry. Despite the low conversion efficiency at the present time, the ability to convert heat from solar radiation and various chemical/nuclear reaction processes also makes efficient thermoelectric materials a prominent candidate for power generation in the near future [1,2]. In general, the dimensionless thermoelectric figure of merit (ZT) is proportional to the ratio of the electrical conductivity to the thermal conductivity. Hence, major research efforts have been focused on developing materials that could maximize this ratio, leading to the so-called "phonon glass electron crystal" concept [3]. However, increasing the electrical conductivity without increasing carrier-assisted heat conduction is challenging. Particularly, detailed engineering of quantum structures is often required. Therefore, reducing the lattice thermal conductivity without altering the electrical properties provides a relatively practical means to achieve high ZT. Advanced nano-fabrication technologies offer new opportunities to tailor phonon transport via the classical size effect, which manifests when the structural dimensions of the materials are smaller than the phonon mean free path, ~250-300 nm [4,5]. For example, superlattices using atomic layer deposition have been demonstrated to exhibit enhanced ZT in various material systems [6,7]. Recent studies have also shown that a single silicon nanowire (SiNW) displays a reduced thermal conductivity of 1.6 W/m·K at room temperature (compared to 140 W/m·K for bulk), greatly boosting its ZT to nearly unity [8,9]. In this context, it is highly desirable to develop bulk-sized nanostructured materials that show significant reductions of phonon thermal conductivities using simple and scalable fabrication processes. Herein, we demonstrate large-area, vertically-aligned silicon nanowires of various lengths fabricated on silicon substrates using a silver-induced, electroless-etching method [10]. The fabrication process can be applied to both n- and p- type nanowires, making them ideal components for thermoelectric devices. A schematic of the proposed device is shown in Fig. 1, where the inset shows the scanning electron microscopic (SEM) image of a fabricated SiNW sample which occupies almost one-half thickness of a wafer. The measured thermal conductivity of the nanowire composites is reduced by up to 43%, compared to that of bulk silicon. Theoretical models based on the series thermal resistance and phonon radiative transfer clearly dictate the reduction of thermal conductivity not only due to the increased air fraction, but also the nanowire size effect.

#131401 - $15.00 USD Received 13 Jul 2010; revised 3 Sep 2010; accepted 3 Sep 2010; published 9 Sep 2010

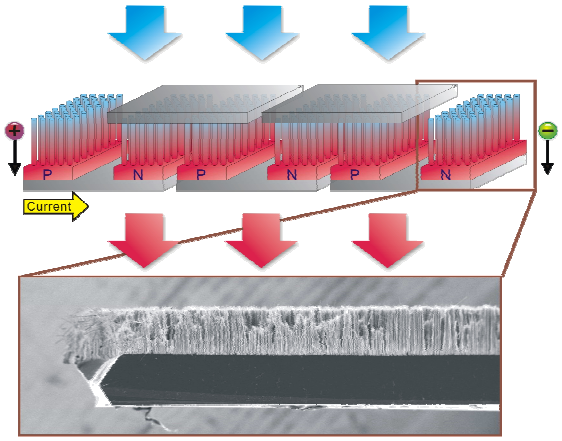

Fig. 1. The schematic of a proposed thermoelectric device using n- and p-type silicon nanowire arrays fabricated on silicon substrates. The inset shows a scanning electron micrograph of a fabricated silicon nanowire composite.

2. Experimental and measurement

Metal-induced electroless-etching of silicon in a hydrofluoric acid (HF) solution has been widely investigated in the past decade. The technique does not significantly depend on the doping type of silicon substrates, and therefore can be implemented on both p- and n- type wafers. Moreover, the synthesized nanowires also exhibit the same axial crystallographic orientations and doping levels as the original wafer, making the control of the electrical properties of SiNWs straightforward. Since the formation of nanowires involves metal-particle-induced catalytic oxidation and dissolution of silicon, the side-wall surface profile is rather rough, which is beneficial for decelerating phonon transport due to additional boundary scattering. In this work, the silicon nanowires were prepared on commercially available p-type (100) silicon substrates with a resistivity between 10 and 100 Ω-cm and a thickness of 650 μm. The six-inch substrates were first cut into quarters and, after standard cleaning steps, immersed in the $AgNO_3$ and HF solution to initiate the electroless metal deposition. During the process, the silver ions captured electrons from the silicon valence band, forming silver dendrite and meanwhile oxidized the silicon. The silicon dioxide was then etched away by the HF solution, causing silver particles to sink into bulk silicon. The remaining silicon therefore formed nanostructures such as holes or wires that depend on the distribution and density of silver particles. At the end of etching process, the samples were dipped in a HNO_3 solution to remove the silver residues.

The nanowire composites were prepared on 650-μm-thick substrates with various nanowire lengths: 35, 60, 130, 143, 215, and 320 μm. The 35- and 60-μm-long nanowire samples were etched in the $AgNO_3$/HF solution with a concentration of 0.02M/5M at room temperature for 2.5 hours and 5.5 hours, respectively. The rest of the samples were etched with $AgNO_3$/HF concentrations of 0.03M/6.5M, 0.04M/6.5M and 0.05M/6.5M for 24 hours. Here, different etching treatments were adapted to obtain a large span of nanowire lengths. In particular, the concentration of the $AgNO_3$ solution was increased to assure the supply of silver and to avoid the lateral etching due to the long etching time. Figure 2(a) and 2(b) show the tilted, 45° scanning electron microscopic (SEM) images for the 35- and 215-μm-long nanowire samples, respectively. The nanowires with high aspect ratios appear to be bundled in groups due to the electrostatic force. The resulting surface morphology depends on the etching conditions, as discussed previously by Peng *et al.* [11]. Figure 2(c) and 2(d) are the cross-sectional views of 2(a) and 2(b), respectively, where the nanowires are relatively uniform in length. Figure 2(e) shows the widths of individual nanowires, which are on the order of 200 nm and therefore, smaller than the phonon mean free path of ~250-300 nm. Moreover, the length variations of the nanowire composites have been quantified via the cross-sectional

#131401 - $15.00 USD Received 13 Jul 2010; revised 3 Sep 2010; accepted 3 Sep 2010; published 9 Sep 2010

SEM images: 35 μm ± 2.2%, 60 μm ± 4.3%, 130 μm ± 4.2%, 143 μm ± 4.2%, 215 μm ± 1.3%, and 320 μm ± 3.1%. Finally, Fig. 2(f) shows a top-view photograph of a fabricated SiNW sample, where the nanostructured surface appears to be black due to reduced optical reflection and strong absorption. This is reminiscent of the broadband anti-reflection properties of silicon nanotips prepared by using a self-masked dry etching technique [12].

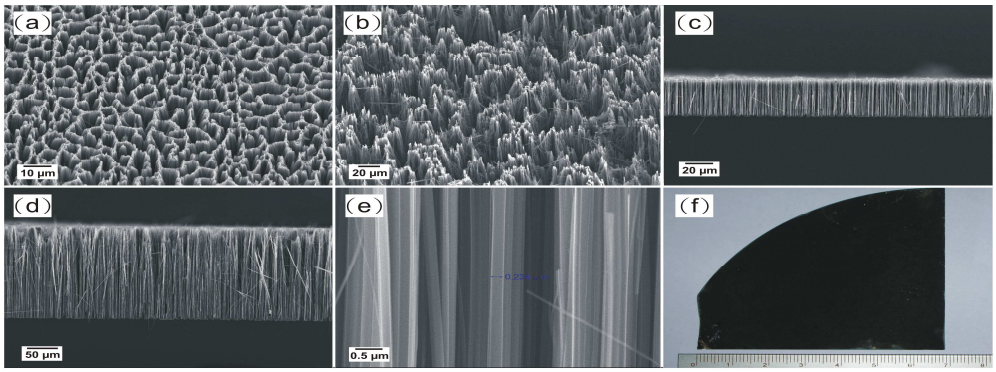

Fig. 2. Scanning electron micrographs of fabricated silicon nanowires (SiNWs): (a) a tilted 45° top view of the 35-μm-long SiNWs, (b) a tilted 45° top view of the 215-μm-long SiNWs, and (c) and (d) the cross-sectional images of (a) and (b), respectively, where the SiNWs are very uniform in length. (e) The magnified image of (c), where the widths of individual nanowires are on the order of 200 nm. (f) Photograph of SiNW arrays fabricated on one-quarter of a 6-inch silicon wafer.

Although there are several methods to measure the thermal properties of solids [13,14], only a few are suitable for measuring the effective thermal conductivities of nanostructure composites. Recently, a hot-disk thermal-constant analyzer based on a transient plane source method has been used to study porous sintered nickel materials [15], silver nanowire/organic phase change material (PCM) composites [16], and carbon nanotubes [17]. Therefore, in this work, the Hot-Disk 2500 thermal-constant analyzer was employed to measure the effective thermal conductivities of silicon nanowire/air composites including the substrate. The experimental setup is schematically shown in Fig. 3. Among the available modules of the hot-disk analyzer, the slab module is designed to measure moderately or highly conducting materials of thin slab samples. It is assumed that the samples are infinite at the plane parallel to the sensor surface (xy-plane). Thus, Δp, which is defined as the shortest distance from the sensor edge to the free surface, must be larger than the probing depth calculated by $\sqrt{4\kappa t}$ [18]

$$\Delta p \geq \sqrt{4\kappa t}, \tag{1}$$

where κ is the thermal diffusivity and t is the measuring time. As this condition is satisfied, the thermal wave does not reach the horizontal boundaries of the sample during the transient recording. The sample dimensions in the xy-plane therefore could be assumed infinite. In this work, the sensor number was 4922 with a radius of 1.46 cm, and the sample size was one-quarter of a 6-inch silicon wafer. Therefore, Δp is ~2.35 cm. Since κ is 0.9 cm^2/s and the measuring time is 1.2 sec, the calculated probing depth is ~2.1 cm which satisfies Eq. (1). Nevertheless, the thickness of a thin slab sample cannot be ignored. Since the introduced heat could be reflected multiple times inside the sample, a concept of image heat sources is introduced [18]. The reflected heat from the vertical boundary is treated as heat coming from the image heat sources, such that the thermal conductivity of a thin slab sample could be properly calculated. It is important to note that the slab thickness of various silicon nanowire composites including the substrate is set to be 650 μm, which corresponds to the distance between adjacent image heat sources. In other words, the heat reflection at the interface

#131401 - $15.00 USD Received 13 Jul 2010; revised 3 Sep 2010; accepted 3 Sep 2010; published 9 Sep 2010

between the nanowire composite and the substrate is not taken into account. The justification will be provided in the next section when the phonon transfer model is discussed.

Fig. 3. The schematic of the experimental setup using a Hot-Disk 2500 thermal-constant analyzer based on a transient plane source method.

As shown in Fig. 3, during the measurement, the hot-disk sensor is sandwiched between two samples that have the same area and nanowire lengths, while the substrate side of the samples is thermally insulated. The calibration is performed by measuring an aluminum bulk which has a known thermal conductivity. The sensor is made of Nickel (Ni) in the shape of a double spiral due to its high temperature coefficient of resistivity. The double-spiral-shaped sensor consists of four electrical connections: two for carrying the heat current and the other two for sensing. Hence, the sensor acts as both, a heat source for increasing the temperature of the samples and a thermometer for measuring the temperature increment. The thermal conductivity can then be calculated from the recorded temperature increase as a function of time. The principle of a hot-disk measurement is discussed in detail in Ref [18]. The measured thermal conductivities of the nanowire composites on the silicon substrate are summarized in Table 1. The corresponding reduction factors are 17%, 29%, and 43% for the 60-μm, 215-μm and the 310-μm long nanowires, respectively, compared to bulk silicon. In general, the experimental data indicates that the thermal conductivities monotonically decrease with the length of nanowires. In Sec. IV, we show that the measured data can be explained by the increased air fraction and also the nanowire size effect.

Table 1. Measured Thermal Conductivities of Silicon Nanowire Composites

Length of SiNWs (μm)	bulk	35	60	130	143	215	320
Effective thermal conductivity (W/m.K)	138	120	115	111	107	98	79

3. Calculation methods

Theoretical models based on the series thermal resistance and phonon radiative transfer were employed to investigate the reduction of thermal conductivity due to both effects mentioned above. The series thermal resistance of the silicon nanowire composite was calculated using the following equation:

$$\frac{d_1 + d_2}{k_{eff} A_1} = \frac{d_1}{k_1 A_1} + \frac{d_2}{k_2 A_2}, \tag{2}$$

where d_1, k_1, and A_1 are the thickness, thermal conductivity, and cross-sectional area of the silicon substrate, respectively; d_2, k_2, and A_2 are those of a nanowire in a unit cell; and k_{eff} is the effective thermal conductivity of the composite including substrate. By setting $k_1 = k_2$, the reduction in k_{eff} is solely due to the air fraction arising between two different cross-sectional areas. Here, the air volume ratio is defined as the etched silicon volume (air gaps) to the

#131401 - $15.00 USD Received 13 Jul 2010; revised 3 Sep 2010; accepted 3 Sep 2010; published 9 Sep 2010

combined nanowire volume including air gaps, which is estimated using the following expression:

$$\text{air volume ratio}(\%) = \frac{\Delta w}{w}\frac{l}{\Delta l}, \tag{3}$$

where w and l are the total weight and sample thickness before etching, Δw is the weight difference before and after the etching process, and Δl is the etching depth. The air volume ratio is estimated to be 30% for the 35-μm long and slightly increased to be 45% for the 215-μm long samples due to the lateral etching. Therefore, the ratio is set to be 40% in our simulation. Although the thermal conductivity of the nanowire composites reduces with the increase of air fraction, it is not desirable for thermoelectric materials, since the electrical conductivity also reduces concurrently. The nanowire size effect, on the other hand, can reduce heat transfer without compromising electron conduction.

The Boltzmann transport equation, which is often used to derive heat conduction properties, was employed to study the size effect in nanostructures [19–21]. This approach treats phonon transport in terms of particle propagation and reflection at interfaces. The Boltzmann transport equation is written as:

$$\frac{\partial f}{\partial t} + v \cdot \nabla f = \left(\frac{\partial f}{\partial t}\right)_{scat}, \tag{4}$$

where f is a time-dependent probability distribution function of phonons, which depends on particle position, time t, and phonon group velocity v. The right hand side of Eq. (4) denotes a scattering term, which arises from the collision between particles. As the collisions tend to relax the system to equilibrium, the scattering term can be rewritten using a relaxation time approximation:

$$\left(\frac{\partial f}{\partial t}\right)_{scat} = \frac{f_0 - f}{\tau}, \tag{5}$$

where f_0 is the Bose–Einstein distribution of phonons, which depends on the local equilibrium temperature, and τ is the relaxation time.

As phonons are treated as particles, the energy flow per unit time, per unit area is defined as the phonon intensity, which can be obtained by multiplying the phonon number per unit volume with the energy of a single phonon and the group velocity. Therefore the phonon intensity has the following expression:

$$I(\theta, \phi, x, y, t) = \frac{1}{4\pi}\sum v f \hbar \omega D(\omega), \tag{6}$$

where θ is the azimuthal angle and ϕ is the polar angle in a spherical coordinate system, and $D(\omega)$ is the phonon density of states as a function of the phonon frequency ω. The product of $D(\omega)$ and the distribution function f on the right hand side of Eq. (6) is the number of phonons per unit volume. We note that the phonon dispersion relation is not taken into account here due to the incoherent nature of phonon transport in nanostructures. Several studies have shown that diffusive interface scattering is the dominant factor of phonon transport in low-dimensional systems, where the coherence of phonons may be destroyed after a few scattering events [22,23]. Since the silicon nanowires fabricated by the electroless metal deposition have rough side-walls, the approximation made in this approach is justified.

By incorporating Eq. (5) and (6) to Eq. (4), the Boltzmann transport equation can be simplified into a two-dimensional equation of phonon radiative transfer (EPRT) to calculate the phonon intensity, which is expressed as:

#131401 - $15.00 USD Received 13 Jul 2010; revised 3 Sep 2010; accepted 3 Sep 2010; published 9 Sep 2010

$$\cos\theta\frac{\partial I}{\partial x}+\sin\theta\cos\phi\frac{\partial I}{\partial y}=\frac{\frac{1}{4\pi}\int_0^{2\pi}\int_0^{\pi}I(\theta,\phi,x,y)\sin\theta d\theta d\phi-I_0}{\Lambda}, \tag{7}$$

where Λ is the phonon mean free path, which is independent of frequency, and I_0 is the equilibrium phonon intensity which has a spatial dependence. The EPRT treats phonon transport as radiation during ballistic heat transport and assumes that phonons, as the wave packets of energy, behave identically to photons. The integrals in (7) can then be approximated by a discrete ordinate method with appropriate weighting functions. Here, an S_4 method with twelve direction cosines and corresponding quadrature weights is employed. Therefore, the EPRT becomes a partial differential equation. The air is assumed to be adiabatic and isothermal boundary conditions are set along the propagation direction.

$$x=0 \qquad I^{+}=I\left(T_H\right), \tag{8}$$

$$x=L \qquad I^{-}=I\left(T_L\right), \tag{9}$$

where I^+ and I^- represents the forward and backward phonon intensity, respectively. By assuming a constant specific heat C, the effective temperature is obtained as:

$$T(x,y)=\frac{4\pi I(x,y)}{C|v|}, \tag{10}$$

where I represents the phonon intensity at local equilibrium at each position solved by Eq. (7). In the calculations, we set $C = 0.93 \times 10^6$ J/m^3.K, $v = 1804$ m/s, and $\Lambda = 260$ nm. The average heat flux q is obtained by:

$$q=\frac{1}{L}\int_0^{L}q_x(x,y)dy, \tag{11}$$

where L is the propagation length and q_x being the local heat flux obtained from the phonon intensity. q_x can be expressed as:

$$q_x(x,y)=\sum_m\sum_n I(x,y,\theta,\phi)\cos\theta w_n w_m, \tag{12}$$

where w_m and w_n are weighting functions of the direction cosines in the S_4 method. In the end, the effective thermal conductivity is obtained by:

$$k=\frac{qL}{T_H-T_L}. \tag{13}$$

Finally, we note that in the series thermal resistance model, the reduced thermal conductivity of a nanowire composite is attributed to the increased air fraction, while in the EPRT, the reduced thermal conductivities arise from both the air fraction and the size effect. As the EPRT is the microscopic description of phonon transport, the simulation results should be consistent with the macroscopic model such as the series thermal resistance, which is indeed verified for bulk materials.

4. Results and discussion

The EPRT model was established to calculate the effective thermal conductivity of nanowire composites with various lengths on a silicon substrate. The surface roughness of silicon nanowires is taken into account by the boundary conditions which describe the phonon transport behavior at interfaces. To determine a proper boundary condition, we adopted the approach proposed by Ziman [24], where an interface specularity parameter ρ is defined as:

#131401 - $15.00 USD Received 13 Jul 2010; revised 3 Sep 2010; accepted 3 Sep 2010; published 9 Sep 2010

$$\rho = \exp(-\frac{16\pi^3\delta^2}{\lambda^2}), \tag{14}$$

where δ is the characteristic interface roughness. The characteristic phonon wavelength defined as $\lambda = hv_s/k_BT$ is about 1 nm at room temperature, where h is the Planck constant, v_s is the sound speed of the material and k_B the Boltzmann constant. ρ is a number between 0 and 1, where $\rho = 1$ represents the specular reflection of phonon transport at smooth interfaces, and $\rho = 0$ a totally diffuse boundary condition. Any number in between represents a partially specular and partially diffuse scattering condition. Figure 4(a) and 4(b) illustrate the specular and diffuse reflections of phonon transport occurring at smooth and rough interfaces, respectively. The specular boundary condition ($\rho = 1$) means that all phonons are reflected following the Fresnel law of reflection, while a totally diffuse boundary condition ($\rho = 0$) means that all the phonons are reflected to random directions with equal probabilities when encountering a boundary. For silicon nanowires obtained by the electroless etching method, the interface roughness is about 1-5 nm [8], hence, the calculated specularity parameter ρ is nearly zero, justifying the use of a totally diffuse boundary condition. Studies have also shown that the totally diffuse boundary condition can well describe the heat conduction of a nanowire [25]. Moreover, it is worth to note that the specular reflection of the EPRT model results in heat transfer properties of bulk material due to phonon momentum conservation (and hence converges to the series thermal resistance model). As shown in Fig. 4(c), the simulation unit cell comprises 25 nanowires on a substrate with a width of 210 nm and a spacing of 140 nm. The length of each nanowire is 35 ± 5 μm, which gives rise to an air volume ratio of ~40%. The total propagation length is 650 μm including the thickness of the silicon substrate. We design the length variation based on a series generation of random numbers in order to take into account the fluctuation of etch rates in the vertical direction. Figure 4(d) shows the calculated temperature gradient for 35 μm nanowire composites with and without the etching length variation (± 5 μm) based on the EPRT with a totally diffuse boundary condition. Due to the length variation, the interface between the nanowire composite and the silicon substrate cannot be strictly defined. As a result, the averaged temperature gradient near the interface varies smoothly, which is in contrast to the slope discontinuity at the clear interface when the length variation is not considered. The smooth temperature gradient implies minimal phonon reflection at the nanowire/substrate interface in a manner similar to photon propagation through media with graded refractive index profiles [26]. We believe that the calculation result justifies the neglected heat reflection at the nanowire/substrate interface when using the transient plane method.

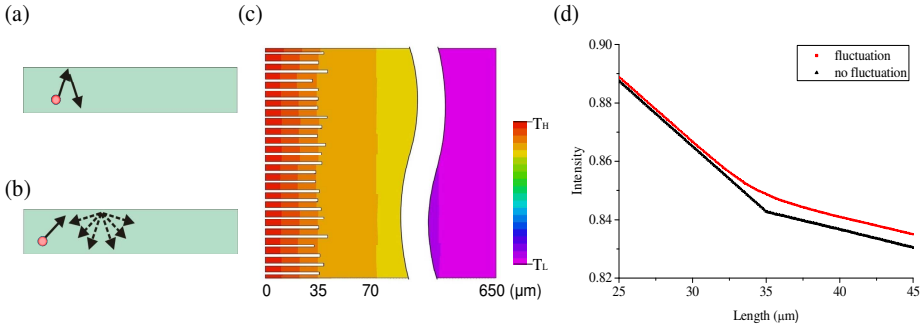

Fig. 4. (a) The schematic diagrams of heat transfer at boundary with a specular reflected boundary condition and (b) a diffuse boundary condition. (c) The simulation unit cell comprises 25 nanowires with a length of 35 ± 5 μm on the silicon substrate. The total propagation length is 650 μm. (d) The calculated temperature gradients near the nanowire/substrate interface for 35-μm-long nanowire composites with and without the etching length fluctuations.

#131401 - $15.00 USD Received 13 Jul 2010; revised 3 Sep 2010; accepted 3 Sep 2010; published 9 Sep 2010

Next, the reduced thermal conductivities of nanowire composites on the silicon substrate are calculated as a function of the nanowire lengths using both the series thermal resistance and the EPRT models. As mentioned previously, the former considers the reduction due to air gap only, while the latter takes into account both the air gap effect and boundary scattering of nanowires. Figure 5(a) shows the calculated results with various air volume ratios of 30%, 40%, and 50% using both models, where the black squares denote the experimental values from Table 1 with estimated length variations as error bars. The blue lines and symbols denote the calculated thermal conductivities from the series resistance model, while the red denote those from the EPRT model. Since the air volume ratio has been experimentally determined to be near 40%, it appears that the series resistance model overestimates the effective thermal conductivities of silicon nanowire composites on the substrate. Hence, we believe that classical size effects are involved in decelerating the heat conduction.

In Fig. 5(b), we fixed the air volume ratio to be 40% and the wire width 210 nm. The calculated thermal conductivities based on the EPRT model agree well with the measured values for the 35-μm and 60-μm long samples. However, we noted that the measured thermal conductivities of other samples with relatively long wires are not as low as those predicted by the EPRT. This inconsistency is possibly due to the following reasons. First, as seen in Fig. 2(a) and 2(b), the long nanowires have very high aspect ratios and hence tend to be bundled together which may diminish the classical size effect. The phenomenon aggravates with the increase of nanowire lengths in which the air fraction also increases due to the lateral etching. Secondly, the width of nanowires, which depends on the distribution and density of silver particles, could be totally random. The variation in width could be as high as a few hundred nanometers, giving rise to fluctuations in the macroscopic thermal conductivities. Therefore, in Fig. 5(b), we also plot the calculated steady-state thermal conductivities for nanowires with widths of 315 nm and 105 nm (210 nm ± 50%) in dashed and dash-dotted lines, respectively. By taking in to account the width variation, the calculated thermal conductivities are close to those measured in experiments. We also note that the thermal conductivity decreases rapidly when the width is reduced beyond the phonon mean free path. Hence, as seen in Fig. 5(b), the dash-dotted line descends much faster than the dashed line, although both have the same width variation (50%) from 215 nm.

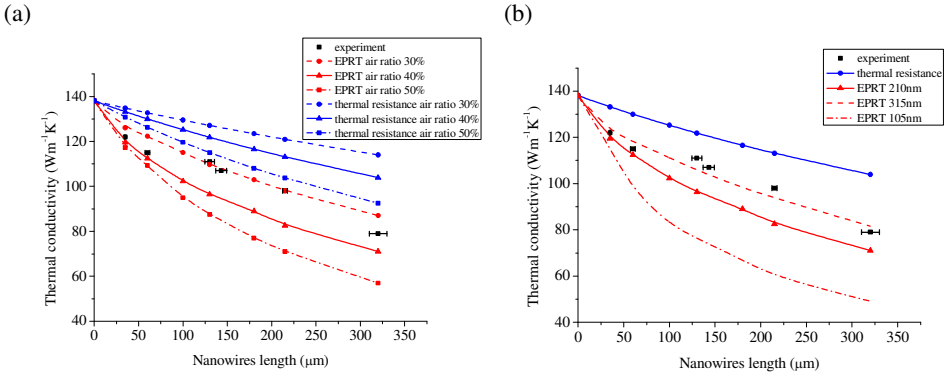

Fig. 5. The effective thermal conductivities of silicon nanowire composites including the substrate are calculated as a function of the nanowire length using both the series thermal resistance model (blue lines/symbols) and the EPRT model (red lines/symbols): (a) for air ratios of 30%, 40%, and 50%, and (b) for different nanowire widths of 315 nm (dashed line), 210 nm (solid line) and 105nm (dash-dotted line), where the air ratio is fixed at 40%. In both plots, the measured thermal conductivities are shown in black squares with length variations as error bars.

#131401 - $15.00 USD Received 13 Jul 2010; revised 3 Sep 2010; accepted 3 Sep 2010; published 9 Sep 2010

5. Conclusion

In conclusion, we have fabricated large-area silicon nanowire composites with various etching lengths using a silver-induced electroless-etching method. The fabrication technique is applicable to both wafer types and is independent of doping levels, which is ideal for controlling the electrical properties of nanowires. We show that the measured thermal conductivities of silicon nanowire composites are reduced by as much as 43% compared to that of bulk silicon. Theoretical calculations based on the phonon radiative transfer model confirm the reduction of thermal conductivities due to both air and size effects. Although the thermal conductivity decreases with the increase of nanowire length, long nanowires tend to diminish the classical size effect due to bundling. Therefore, our results suggest that silicon nanowire composites with a low air volume ratio and wire widths much smaller than the phonon mean free path are promising thermoelectric materials for achieving the true "phonon glass, electron crystal" concept.

Acknowledgments

The authors thank Prof. H. C. Kuo at the Department of Photonics, National Chiao Tung University in Taiwan for technical support. This work is founded by National Science Council in Taiwan under grant number 96-2221-E-009-095-MY3 and 97-2120-M-006-009.

#131401 - $15.00 USD Received 13 Jul 2010; revised 3 Sep 2010; accepted 3 Sep 2010; published 9 Sep 2010